Anal. Methods Environ. Chem. J. 8 (2) (2025) 5-25

AMECJ

Research Article, Issue 2
Analytical Methods in Environmental Chemistry Journal
Journal home page: www.amecj.com/ir

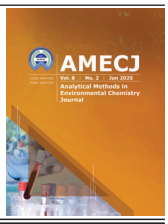

Utilization of maize pith powder as a cost-effective adsorbent for the removal and analysis of Crystal Violet from aqueous solutions before determination by UV-Vis spectrophotometry

Smail Imame[a], Hafssa Atlas[a], Mohamed Sadoq [a], Khaoula Loukili [a], Mohammed Legsaier[a], Mohamed Karim El Bakkali [a], and Fatima Boukhlifi [a,]**

[a]Laboratory of Chemistry and Biology Applied to the Environment, URL-CNRST-N◦13, Faculty of Sciences, Moulay Ismail University, Meknes 50050, Morocco

ARTICLE INFO:

Received 11 Feb 2025
Revised form 20 Apr 2025
Accepted 24 May 2025
Available online 29 Jun 2025

Keywords:
Crystal Violet,
Analysis,
Adsorption,
UV-Vis spectrophotometer,
Maize pith powder

ABSTRACT

The removal and analysis of crystal violet (CV; Triarylmethane dye) from water samples using maize pith (MP) powder was demonstrated to assess its potential as an economical adsorbent. The optimum parameters for biomass biosorption, with an initial dye concentration of 30 mg L^{-1}, were determined by MP adsorbent (2.5 g L^{-1} biomass, pH 10, temperature 25°C, and contact time 40 minutes). An analytical method based on UV-Vis spectrophotometers was used to analyze the fluids under study and determine the CV dye concentration. A UV-Vis spectrophotometry determined the crystal as a limit of quantification (LOQ) of 0.1 mg L^{-1} and a limit of detection (LOD) of 0.04 mg L^{-1}. The Linear range of the procedure is 0.1 to 30 mg L^{-1}, which guarantees precise and repeatable results (RSD%< 5%). Thermodynamic analysis showed that dye biosorption was exothermic, sporadic, and spontaneous. The Langmuir, Freundlich, Temkin, and Dubinin-Radushkevich models provide a more accurate description of the results. According to the Langmuir equation, the highest biosorption capacity (q_{max}) was 11.90 mg g^{-1}. Given that both the Freundlich parameter 1/n and the Langmuir separation coefficient R_L are smaller than 1, it is clear that CV bioadsorption on MP is beneficial. In addition, there is the pseudo-second-order mechanism. In addition, intraparticle diffusion revealed a boundary layer effect. FT-IR analysis confirmed that different functional groups were responsible for dye binding. Electron microscopic scanning revealed a high degree of porosity at the surface of the biomass, allowing free passage of the dye molecules.

1. Introduction

Economic growth encouraged by intensive industrialization, which began in the last century, has released a variety of pollutants into the environment, many of which are long-lasting. The slow decomposition of these substances poses a significant threat to human health and biodiversity. Growing awareness of water pollution has strengthened the actions taken to combat this problem. The textile industry, which uses large quantities of water during the dyeing process, is one of the leading emitters of liquid effluents. [1]. According to analytical chemistry methods, approximately 50% of the world's dye production is lost during dyeing and disposed of as textile waste [1]. Industrial chemical dyes, which are toxic aromatic substances, represent a significant threat

*Corresponding Author: Fatima Boukhlifi
Email: f.boukhlifi@umi.ac.ma
https://doi.org/10.24200/amecj.v8.i02.1010

to the environment and human health [2]. Crystal violet, frequently used as a dye in the paper and textile industries, is also recognized as a biological and dermatological agent in human and veterinary medicine [3]. It is considered one of the most dangerous because of its resistance to biological degradation, its mutagenic and carcinogenic properties, and its prolonged persistence in the environment. Crystal violet is one of the brightest water-soluble dyes, and low concentrations can cause intense coloration that inhibits photosynthesis. Skin absorption, inhalation, and ingestion can cause severe irritation and painful sensitization [4]. It can also cause intense eye inflammation and kidney failure, leading to cancer and permanent blindness. It is therefore considered biologically potentially harmful [5]. Treating wastewater contaminated by CV before its release into the environment is a crucial research topic. Contaminants can be removed from wastewater using various analytical chemistry methods, including biological oxidation, photocatalytic degradation, ion exchange, chemical precipitation, membrane separation, and chemical adsorption [6-10]. Disadvantages of these methods include reuse, regeneration, and cost. Chemical biosorption has been widely studied to remove pollutants from water (for example, heavy metals and dyes) using solid agricultural waste as adsorbent material [11]. Biosorbents are advantageous because they are cost-effective, environmentally friendly, renewable, and require less treatment time [12]. Various materials, such as coffee black [13], almond shell [14], argan nut shells [15], and pericarp of the glans [16], are being studied as potential biosorbents for removing dyes from aquatic environments.

This research aimed to analyze the ability of maize pith to remove crystal violet from aqueous solutions under various biosorption conditions, such as voltage, pH, duration of biosorption, and quantity of biosorbent. Research into biosorption has also focused on kinetic, isothermal, and thermodynamic mechanisms. Finally, studies have been conducted on how biomass removes and analyzes crystal violet from real wastewater.

2. Materials and methods

2.1. Reagents and Instruments

In this study, the dye examined has a violet hue. It is a triphenyl-based cationic dye commonly referred to as methyl violet, gentian violet, aniline violet, or hexamethyl pararosaniline chloride with the molecular formula $C_{25}H_{30}N_3Cl$ (CAS No: 548-62-9), and its chemical structure is shown in Figure 1 [17]. All experiments used analytical-grade chemicals. Hydrochloric acid (HCl, 99%, CAS No: 7647-01-0) and sodium hydroxide (NaOH, 36.5%, CAS No: 1310-73-2) were acquired from Sigma-Aldrich (Saint-Quentin-Fallavier, France). Table 1 describes the primary features of the dye.

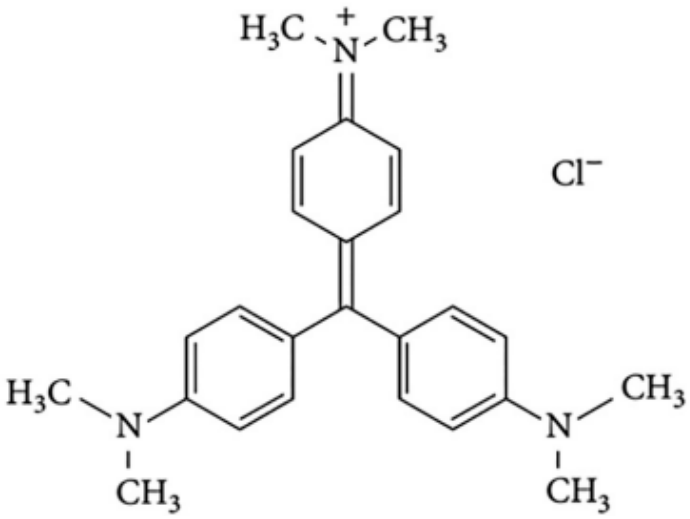

Fig. 1. Chemical structure of crystal violet

Table 1. Physicochemical properties of CV

Parameter	Value
Generic name	Crystal violet
Molecular formula	$C_{25}H_{30}N_3Cl$
Molecular weight	407.98 g mol^{-1}
Absorption maxima	582.0 nm
Type of day	Cationic

2.2. Preparation of biosorbent

Preparing maize pith as biomass involves several stages. Maize pith, the fibrous residue obtained after grinding the heart of the maize stalk, undergoes a multi-stage process. First, it is carefully cleaned several times with hot distilled water to remove impurities. After cleaning, the pith is vacuum-filtered to remove excess wash water. It is then dried overnight for 12 hours at 60°C. Once dried, the marrow is ground using a grinder (brand: FRITSCH, Germany). It is then sieved with a sieve shaker (brand: FRITSCH, Germany), and only particles smaller than or equal to 0.2 mm are retained. The final product is then stored for experimental studies.

2.3. Characterization techniques

Several physicochemical techniques were used to characterize the studied solid, such as X-ray diffraction (XRD), which was performed using a high-resolution X-ray diffractometer (D8-ADVANCE A25, Bruker) equipped with a graphite monochromator and CuKα radiation at a fixed power source (40 kW, 20 mA). Diffraction measurements were conducted with a 2θ angle range of 5-70 degrees. The FTIR spectra were recorded using an FTIR spectrophotometer (model Spectrum, IRAFFINIY-1S) employing the KBr pressed disk technique. The solid is diluted to 5% in KBr, then ground and homogenized to form a fine powder. The finely powdered mixture was compressed into a pellet under high pressure. Spectra were recorded from the solid samples with a resolution of 20 cm^{-1} over the 4000 to 400 cm^{-1} range. UV/Visible spectrophotometry is a qualitative and quantitative analysis method that identifies a chemical species' presence and concentration. For this purpose, the spectrophotometer used is of the type (SHIMADZU-UV 1800), which allows the measurement of the absorbance of a solution at a precise wavelength between 190 nm and 900 nm. The concentrations are deduced from the Beer-Lambert law (A = ε. ℓ.C). The point of zero charge is the pH for which the surface charge of the solid is zero; it was determined by the method of adding the solid [18].

2.4. Adsorbate Preparation

Crystal violet dye (CV) was used as an adsorbent (characteristics presented in Table 1). Firstly, a stock solution of crystal violet (0.1 g L^{-1}) was prepared by dissolving a specific quantity in distilled water. The stock solution was then diluted to obtain the desired concentration.

2.5. Adsorption procedure

All the experiments in this work were carried out in the same experimental set-up, except for the study of the effect of temperature. A water bath was used to set the temperature to the desired value. To determine the optimum experimental conditions for treating a 20 mL of a sample with an initial C_0 concentration of 30 mg L^{-1} dye, The effects of contact time (0–65 min), MP dosage (5–50 g L^{-1}), temperature (25°C–55°C), and pH (2–12) were examined. The pH of the solutions was adjusted using 0.1M NaOH and 0.1M HCl solutions. The suspensions are then stirred until they reach equilibrium. After this time, the supernatant was extracted by centrifugation. The solution was analyzed by UV-visible spectrophotometry at a wavelength of 582 nm (Schema 1). Determining the adsorbed amounts of CV is performed on the calibration line. The adsorbed amounts are calculated using Equation 1 [19].

$$q_{ads} = \frac{(C_0 - C_e).\ V}{m}$$

(Eq.1)

Where C_0 and Ce (mg L^{-1}) are the initial and equilibrium concentrations of the dye, respectively; m is the mass of the solid in g; V is the volume of the dye solution, and q_{ads} is the adsorbed amount per gram of adsorbent in mg g^{-1}.

2.6. Modeling of adsorption kinetics

To interpret the experimental data of CV adsorption on MP, we adopted three kinetic models: pseudo-first-order (PFO), pseudo-second-order (PSO), and intraparticle diffusion.

2.6.1.Pseudo first-order model

The pseudo-first-order model is given by Lagergren, which is expressed by the following Equation 2 [20].After integration with initial conditions, q_{t0} at t=0, Equation 2 is converted to Equation 2a.

$$\frac{dqt}{dt} = K_1(q_e - q_t)$$

(Eq.2)

$$\text{Log}\,(q_e - q_t) = Log(q_e) - \frac{t}{q_e}$$

(Eq.2a)

Where k_1 is the first-order reaction rate constant of adsorption of CV on MP in (min^{-1}), q_e, q_t are the amount of CV adsorbed at equilibrium and at time t in (mg g^{-1}), and t is the contact time in minutes.For the representation of Log (qe-qt) = f(t), we obtain a line that gives k_1 and qe.

2.6.2.Pseudo-second order model

The following expression gives the pseudo-second-order model as Equation 3 [21]. K_2 is the second-order reaction rate constant of adsorption of CV on MP in ($g \times mg^{-1} \times min^{-1}$). After integration, we obtain Equation 4a. The linearization of Equation 4 gives Equation 4b. The representation of t/qt=f(t) allows us to get a line from which we determine k_2 and q_e.

$$\frac{dqt}{dt} = K_2(q_e - q_t)^2$$

(Eq.3)

$$q_t = \frac{K_2 q_e^2 t}{K_2 q_e t + 1}$$

(Eq.4a)

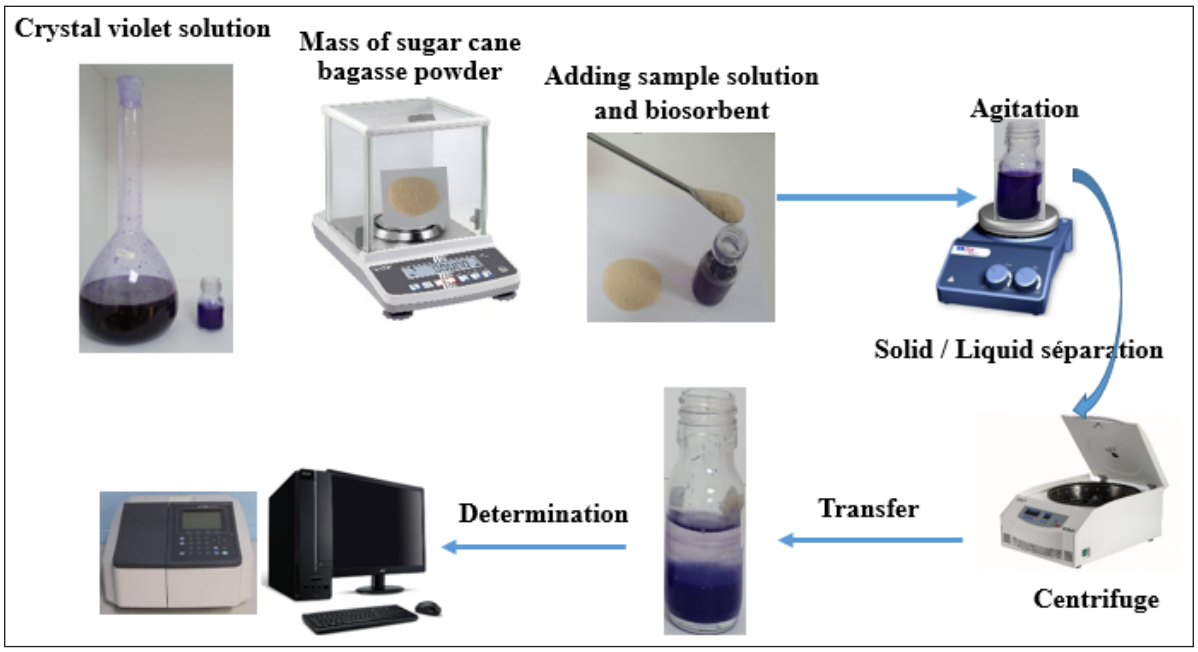

Scheme 1. Procedure for separating CV on PM by UV-visible.

$$\frac{t}{q_t} = \frac{1}{K_2 q_e^2} + \frac{1}{q_e} t$$

(Eq.4b)

2.6.3. Intra-particle diffusion model

The intra-particle diffusion is described by Equation 5, represented by Weber and Morris [22]. K_d is the intra-particle diffusion rate constant, and C is the boundary layer thickness. The representation $q_t = f(t^{1/2})$ allows for calculating k_d and C.

$$q_t = K_d t^{1/2} + C$$

(Eq.5)

2.7. Thermodynamic parameters

The thermodynamic parameters (ΔG°), (ΔH°), and (ΔS°) for the studied system (CV/ MP) were determined and calculated at different temperatures (25°C, 35°C, and 45°C). The adsorption free energy (ΔG°) is calculated according to the standard Gibbs formula defined by Equation 6.

$$\Delta G° = - RT \ln (K_d)$$

(Eq.6)

where K_d is the equilibrium distribution constant defined by $K_d = q_e/ce$. Also, q_e (mg g^{-1}) represents the amount of adsorbed dye at equilibrium and Ce (mg L^{-1}) the residual concentration of the adsorbate at equilibrium.

Equation 7 shows the curve representing the variation of ln (Kd) as a function of 1/T, which can be used to estimate the thermodynamic parameters of the CV's adsorption on the adsorbent.

$$\ln K_c = \frac{\Delta S°_{ads}}{R} - \frac{\Delta H°_{ads}}{RT}$$

(Eq.7)

The values of ($\Delta H°_{ads}$), and ($\Delta S°_{ads}$) are calculated from the slope and intercept of the line obtained by plotting ln (K_c) versus 1/T, respectively.

2.8. Modeling of adsorption isotherms

2.8.1. Langmuir Isotherm Model

The Langmuir model was initially used for systems with monolayer adsorption on the adsorbent surface. This model assumes that all adsorption sites are identical, do not depend on surface coverage, and occur without lateral interaction with the adsorbate molecules (Equation 8a). To determine this model's adsorption parameters, we use the linear form of the Langmuir isotherm, represented by Equation 8b. In addition, the separation factor RL, defined by Equation 8c, is one of the Langmuir isotherm's essential characteristics.

$$q_e = \frac{q_m . K_l . C_e}{1 + K_l . C_e}$$

(Eq.8a)

$$\frac{1}{qe} = \frac{1}{K_l . q_m . C_e} + \frac{1}{q_m}$$

(Eq.8b)

$$R_l = \frac{1}{1 + K_l . C_e}$$

(Eq.8c)

q_m is the maximum adsorbed quantity in mg g^{-1}, and K_l is the Langmuir constant in L mg^{-1}. C_i is the initial concentration of the dye (mg L^{-1}), and K_L is the Langmuir constant (L mg^{-1}). Values of R_L indicate the shapes of isotherms to be either unfavorable ($R_L > 1$), linear ($R_L = 1$), or favorable ($0 < R_L < 1$) [23].

2.8.2. Freundlich Isothermal Model

The empirical model of Freundlich is based on adsorption on heterogeneous surfaces and modulates, as shown in Equation 9a.

$$q_e = K_F . C_e^{1/n}$$

(Eq.9a)

Where, qe is the amount adsorbed at equilibrium, C_e is the residual concentration of the dye at

equilibrium, and n represents the adsorption intensity and indicates whether the adsorption is favorable. If n<1, linear adsorption; if n>1, physical adsorption is favorable [24]. The parameters K_f and n are determined from the linear form of the isotherm by plotting in Equation 9b. The linearization of Equation 9a implies a passage of the terms in logarithmic form as Equation 9c.

$$\text{Log qe} = f(\text{LogCe}) \quad \text{(Eq.9b)}$$

$$\text{Log } (q_e) = \text{Log}(K_f) + \frac{1}{n}\text{Log } (C_e) \quad \text{(Eq.9c)}$$

2.8.3. Temkin Isothermal Model

The derivation of the Temkin isotherm assumes that the decrease in the heat of adsorption is linear rather than logarithmic, as applied in the Freundlich equation. The Equation 10 generally presents the Temkin isotherm [25].

$$q_e = \frac{R.T}{b_T}.\text{ Ln } (A_T.C_e) \quad \text{(Eq.10)}$$

The b_T and A_T are Temkin isotherm constants, R is the perfect gas constant (8.314 Kj mol^{-1}), C_e is the equilibrium concentration of dye ions (mg L^{-1}), and T is the absolute temperature.

2.8.4. Dubinin–Radushkevich Isothermal Model

The Dubinin-Radushkevich (D-R) model is commonly employed to differentiate between physical and chemical adsorption, which was shown in Equation 11 [26].

$$\ln(qe)=\ln(qD)-\beta\varepsilon^2 \quad \text{(Eq.11)}$$

where qe is the equilibrium adsorption capacity (mmol g^{-1}), q_D is the D–R adsorption capacity (mmol g^{-1}), ß (mol^2 kj^{-2}) is the activity coefficient related to the mean adsorption energy, and Ɛ is calculated by Equation 12.

$$\varepsilon = \text{RTln } (1 + \frac{1}{C_e}) \quad \text{(Eq.12)}$$

R represents the universal gas constant (8.314 J/mol K), and T represents Kelvin's absolute temperature (K). Consequently, when we plot $\ln(q_e)$ against $Ɛ^2$, we obtain a linear relationship characterized by a slope of ß and a y-intercept of $\ln(q_D)$. The constant β provides valuable insights into the mean free energy E (kj mol^{-1}) of adsorption per adsorbate molecule when it transitions from an infinite distance in the solution to the solid surface. This value can be computed using the following relationship (Equation 13).

$$E = \frac{1}{\sqrt{2\beta}} \quad \text{(Eq.13)}$$

The E value is commonly used to determine the nature of the adsorption. An ion exchange process generally has an E value of between 8.0 and 16.0 kj mol^{-1}, while a physisorption process generally has an E value of less than 8.0 kJ mol^{-1} [26].

3. Results and discussion

3.1. Characterizations

3.1.1. XRD Analysis

Figure 2 displays the maize pith XRD diffractogram. Lignin, cellulose, and hemicelluloses make up the majority of the MP. Because of the cellulose's semi-crystalline structure found in the biomass, two peaks have been found, with values of 2ɵ approximately 16 and 22. Furthermore, according to Kali et al. [18], the XRD spectrum resembles that of other lignocellulosic waste samples.

3.1.2. FT-IR analysis

The MP solid was analyzed using Fourier transform infrared spectroscopy. The obtained FT-IR spectrum is displayed in Figure 3.

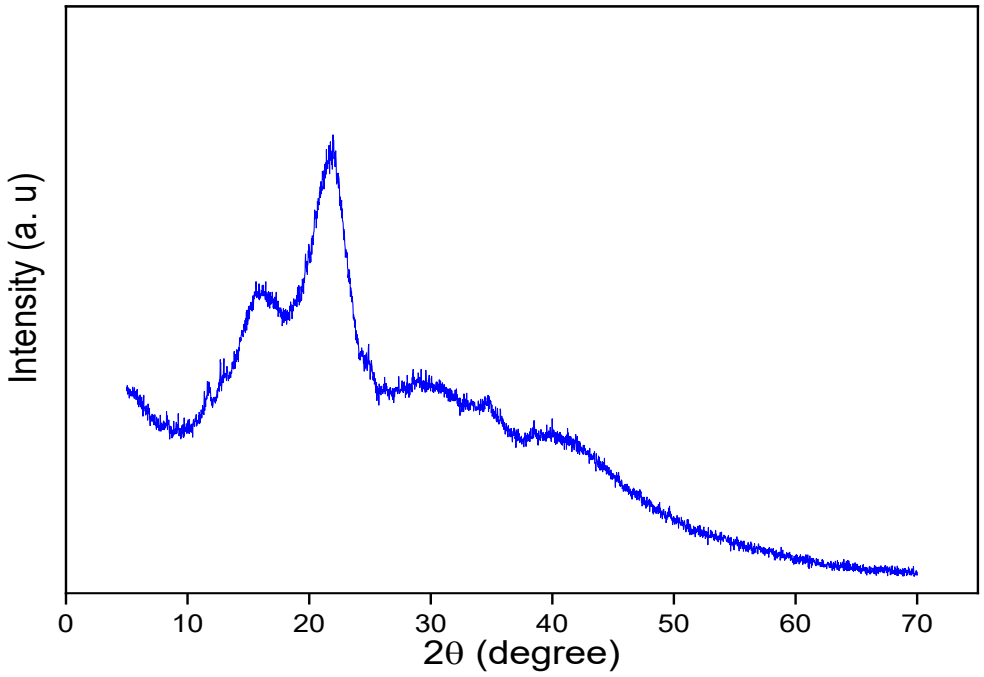

Fig. 2. Powder XRD patterns of MP

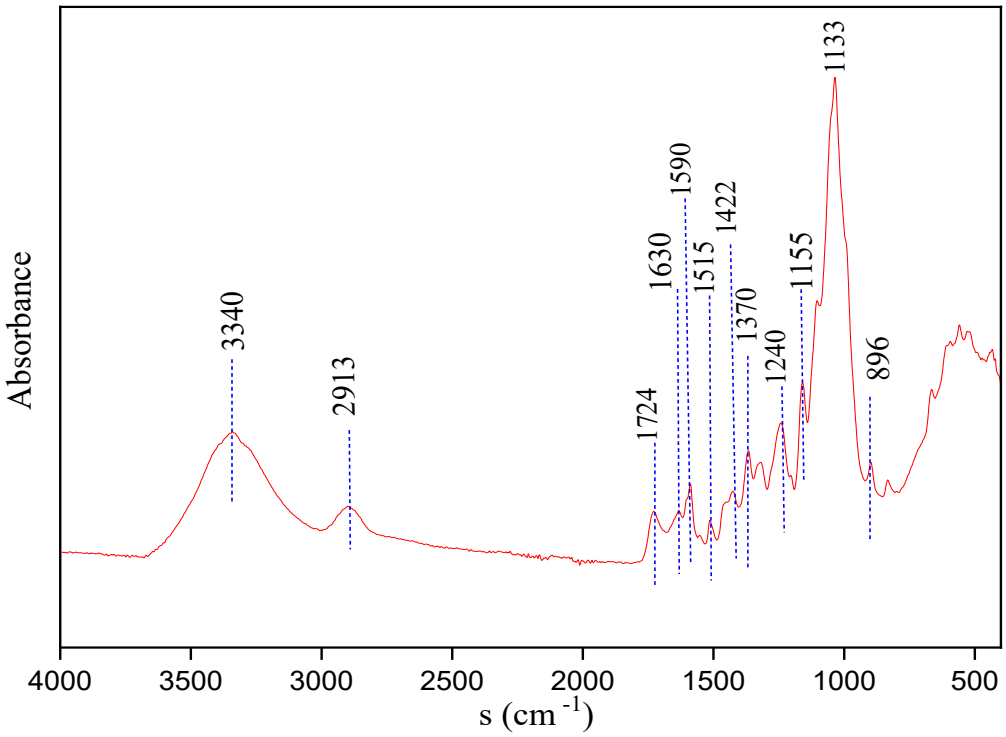

Fig. 3. FT-IR spectra of the MP solid

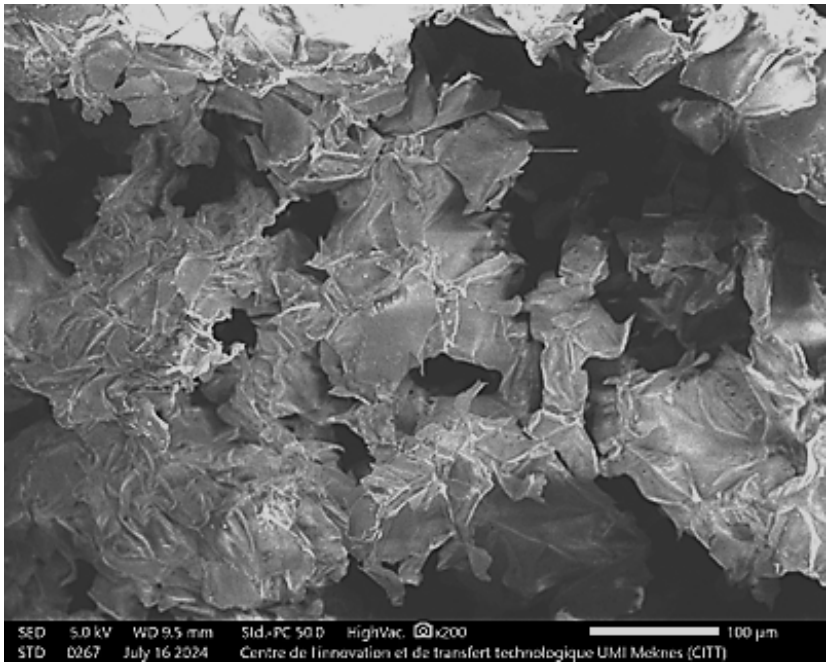

Fig. 4. SEM of raw MP

The following peaks are found in the maize pith powder FTIR spectrum (Figure 3). The band detected at 3340 cm^{-1} is a strong band that is associated with OH groups, which include alcohols, phenols, and carboxylic acids, as well as the NH of amides [27]. The band at 2913 cm^{-1} is linked to asymmetric C–H found in alkyl groups [28]. The band at 1724 cm^{-1} is linked to the stretching vibration of carbonyl groups in MP hemicelluloses [29]. The bands at 1605 and 1515 cm^{-1} were related to the aromatic skeleton vibrations in lignin [30]. The band at 1422 cm^{-1} is related to the –CH variation, and the band at 1630 cm^{-1} is linked to the absorbed water in the cellulose [31], while the band at 1370 cm^{-1} confirms the presence of methoxy-C-O groups in lignin [32]. The band at 1320 cm^{-1} is attributed to the C–H vibration in cellulose [27], and the band at 1240 cm^{-1} is attributed to the elongation vibration of the C-O bonds of aromatic compounds, acid, alcohol, phenol, ether, and ester functions [27]. The skeletal vibration of the C-O-C pyranose ring and the β-glycosidic connections between glucose units in cellulose were linked to the spectrum regions between 1155 and 1033 cm^{-1} and 896 cm^{-1}, respectively [30].

3.1.3.SEM analysis

The SEM micrograph of the MP is shown in Figure 4. This illustration shows that the biomass has an irregular surface and variable porosity. The quasi-spongy structure of the material facilitates the fixation of various pollutants. This morphological characteristic is attributable to the fibres present in this type of lignocellulosic material [16].

3.1.4.Point of zero charge

Seven vials with 50 mL of sodium chloride NaCl (10^{-3} M) each were made for this investigation. By adding NaOH or 0.1M HCl solution, the pH of these vials is brought back to its initial range of 2 to 12. After the initial pH adjustment, 100 mg of the material was added to each vial. The suspensions ‘ ultimate pH was determined after 24 hours of stirring at room temperature. The pHpzc value is calculated using the representation ΔpH = f(pHi). The latter occurs due to the curve and the x-axis intersecting [33]. The representation of ΔpH =f(pHi) allows for determining the pHpzc value, as illustrated in Figure 5. According to Figure 5, the pH value corresponding to the solid surface’s neutrality is 7.15. So, if the pH is above 7.15,

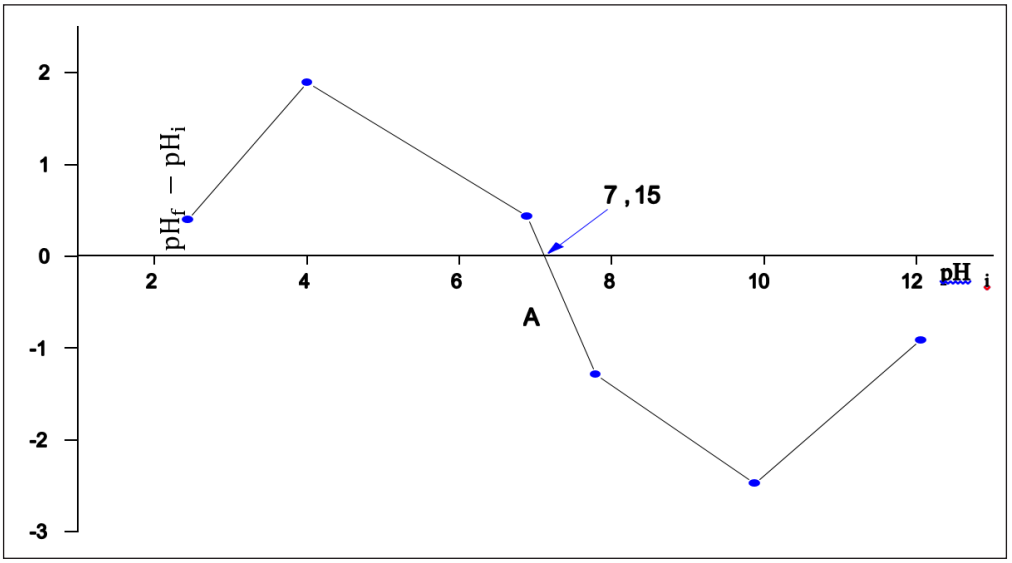

Fig. 5. Point of zero charge of MP

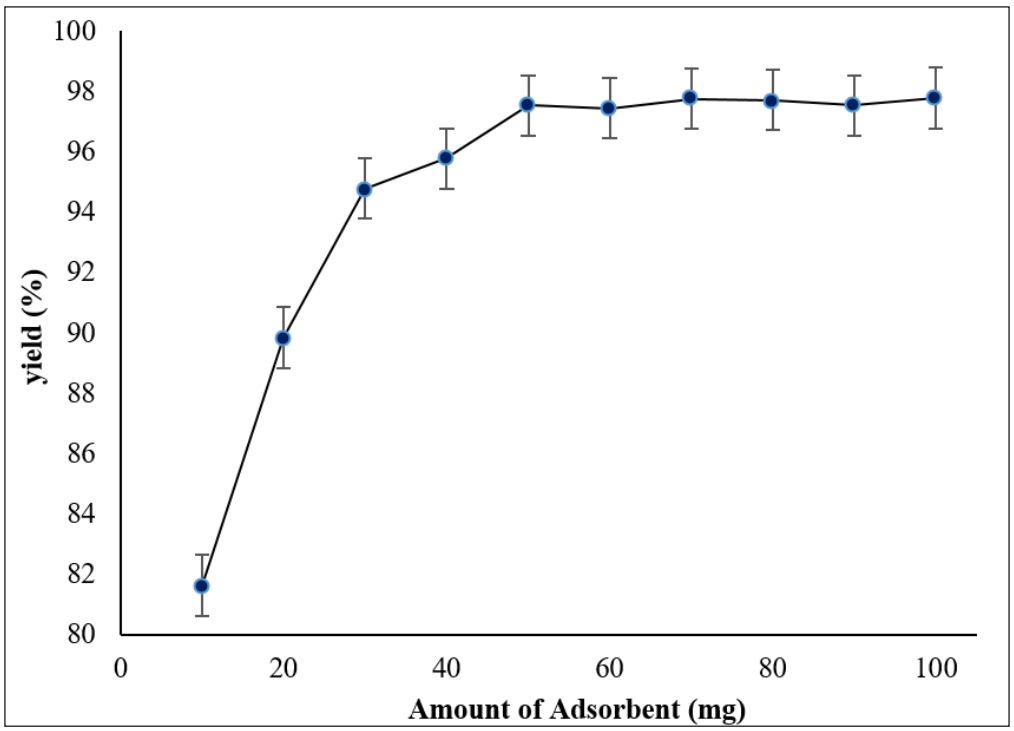

Fig. 6. Percentage of CV removal as a function of MP mass

the solid surface is negatively charged, while a pH below 7.15 results in a positive charge on the surface.

3.2. Study of CV adsorption on MP

Many variables that influence the adsorption phenomenon are examined, such as the adsorbate's mass, the solution's temperature, the duration of the adsorbent-adsorbate contact time, and the solution's initial pH.

3.2.1.Effect of adsorbent mass

Figure 6 shows the impact of the amount of adsorbent on removing CV dye by adsorption.

The findings demonstrate that the dye removal rate increases as adsorbent mass increases. This observation can easily be explained by the correlation between the increase in dye elimination and the increase in the surface area of the adsorbent accessible to the dye molecule, due to the increase in its mass [34]. However, a limit is reached once the mass exceeds 50 mg, which explains why adsorption equilibrium is reached above this quantity of adsorbent (saturation is reached). Thus, an optimum amount of 50 mg of biomass is required to get maximum dye adsorption capacity, enabling 97% of the dye to be eliminated.

3.2.2. Effect of contact time

Figure 7 depicts the investigation of the impact of contact duration on the adsorption of CV dye at different temperatures. The influence of contact time (0-70 min) on CV removal by the MP biosorbent, illustrated in the curves in Figure 7, reveals that biosorption of the CV dye is remarkably rapid. Within the first 40 minutes, a significant increase in biosorption is observed. After this time, a dynamic equilibrium is reached, with maximum adsorption (q_{max}) achieved after 40 minutes of agitation of the solution containing CV dye and BN adsorbent at different temperatures. Thus, the optimum contact time was 40 minutes, with a CV removal rate of up to 97%. It was also observed that the amount of CV adsorbed by the biomass varied slightly with temperature. Increasing temperature influenced the adsorption process, confirming its exothermic nature [35].

3.2.3. Effect of pH

Since the pH affects the charge and ionization of the active groups on the biomaterial's surface, it is crucial to the adsorption process. Through a series of studies, the pH was varied from 2 to 12 for biomass suspensions in 20 mL of dye solution, with a contact period longer than 30 minutes, in order to evaluate its effect on the adsorbent's ability to adsorb the dye. HCl (0.1 M) or NaOH (0.1 M) was added to the suspensions to bring their pH levels to the appropriate levels. Figure 7 displays the findings of the adsorption yield fluctuation as a function of solution pH. Figure 8 illustrates the dependence of CV dye elimination on changes in pH of the solution. Consequently, good dye retention is shown between pH values of 8 and 10, with pH 10 exhibiting especially impressive performance. Retention efficiency is seen to

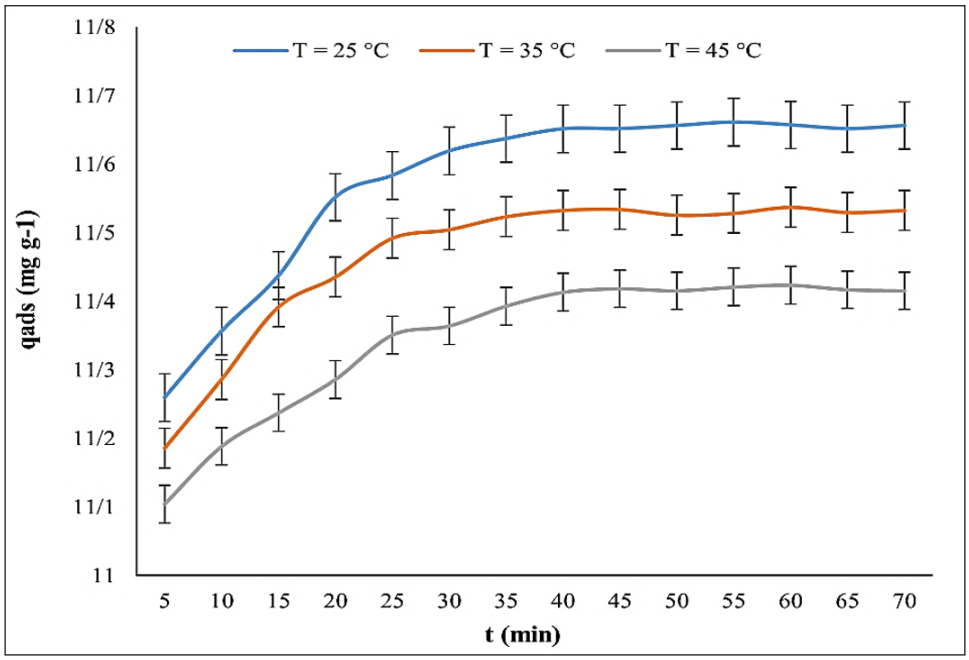

Fig. 7. Effect of contact time on the adsorption of CV dye

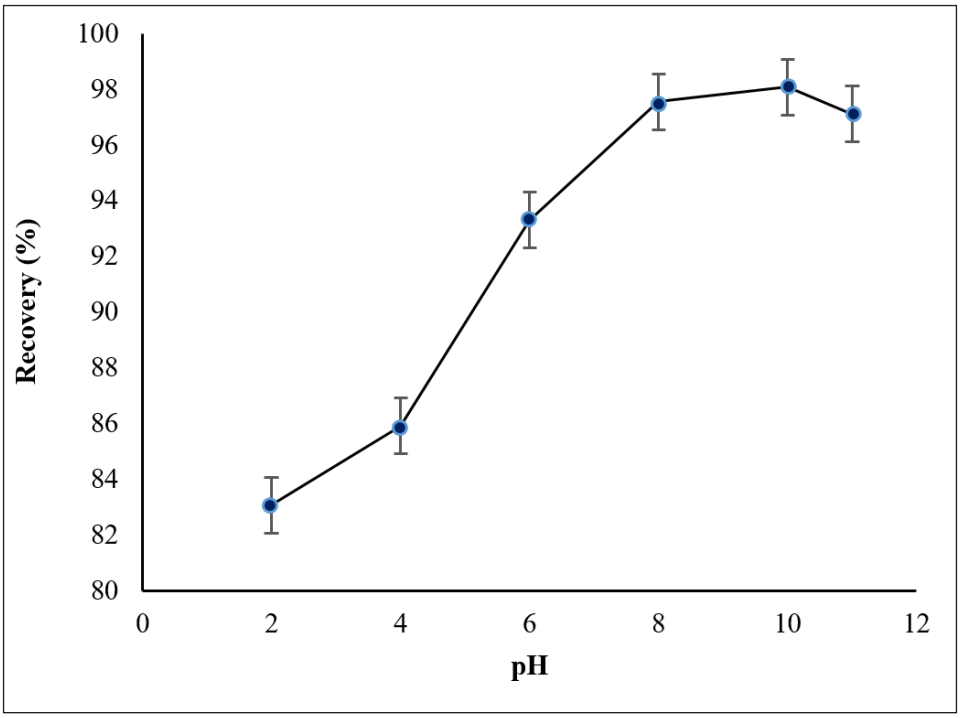

Fig. 8. Influence of pH on CV adsorption

decline at this pH range. The impact of solution pH on these interactions was explained using the pH value of the zero charge point pHpzc. Since the material utilized has a pH_{pzc} of 7.15, the adsorbent's surface is positively charged when the solution's pH is below this value and negatively charged when it is above it. Since the employed dye is cationic and dissolves to release positively charged ions, the primary adsorption forces in the pH range below pH_{pzc} may be hydrophobic and chemical interactions. Electrostatic interactions between the various charges in the suspension and the adsorbent surface may account for the notable dye retention at pH levels above pH_{pzc}. In addition, the solubilization of organic groups present on the surface of the biosorbent at pH values above 10 explains the reduction in dye retention at these same pH values [36].

3.3. Modeling of adsorption kinetics

3.3.1.Pseudo-first-order kinetics

The graph displays the outcomes obtained using the linear Lagergren models. Table 2 presents the kinetic parameters, derived from the gradients and intercepts of the theoretical lines. The results obtained (Fig. 9 and Table 2) show that the experimental data points of this model are not homogeneous; the coefficients of determination R^2 are very different from 1. In addition, the quantities of dye adsorbed during the experiment differ considerably from the calculated values (qcal). As a result, the results of CV adsorption on the adsorbent do not comply with this model.

3.3.2.Pseudo-second order kinetics

The results obtained using Pseudo-second-order linear models are illustrated in the graph (Fig.10). The table shows the kinetic parameters derived from the gradients and ordinates of the theoretical lines. The pseudo-second order model obtained a coefficient of determination (R^2) of 0.99. Furthermore, the calculated value of qe was close to the experimental value of qexp, suggesting that the pseudo-second-order kinetic model was a satisfactory approach to describe the biosorption of CV on MP. In addition, according to Table 2, there was a low pseudo-second order rate constant (K_2) for the CV dye, suggesting that biosorption of CV molecules by MP from aqueous solution occurs rapidly [37].

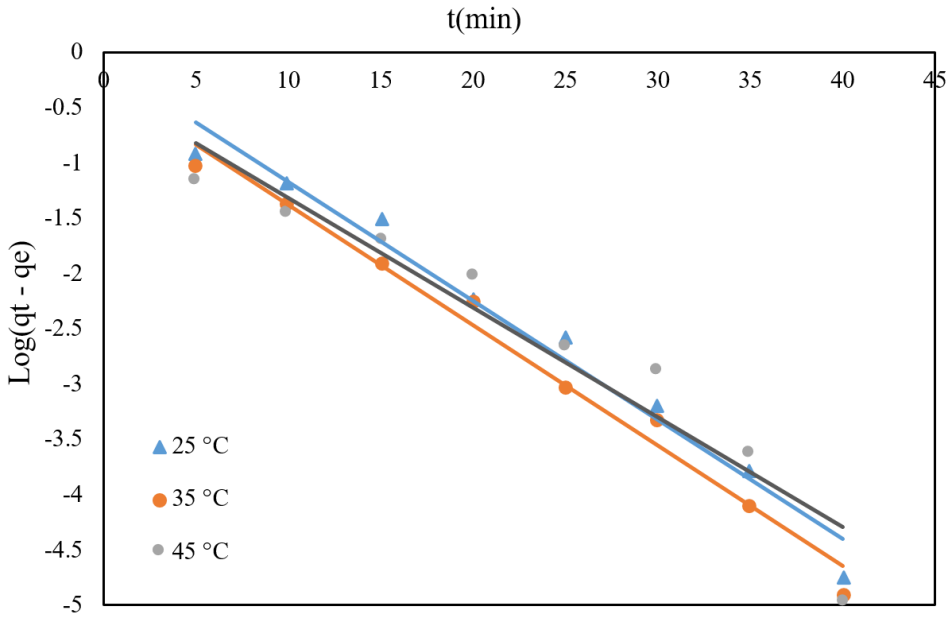

Fig. 9. Plot of the pseudo-first order model of the CV-MP system.

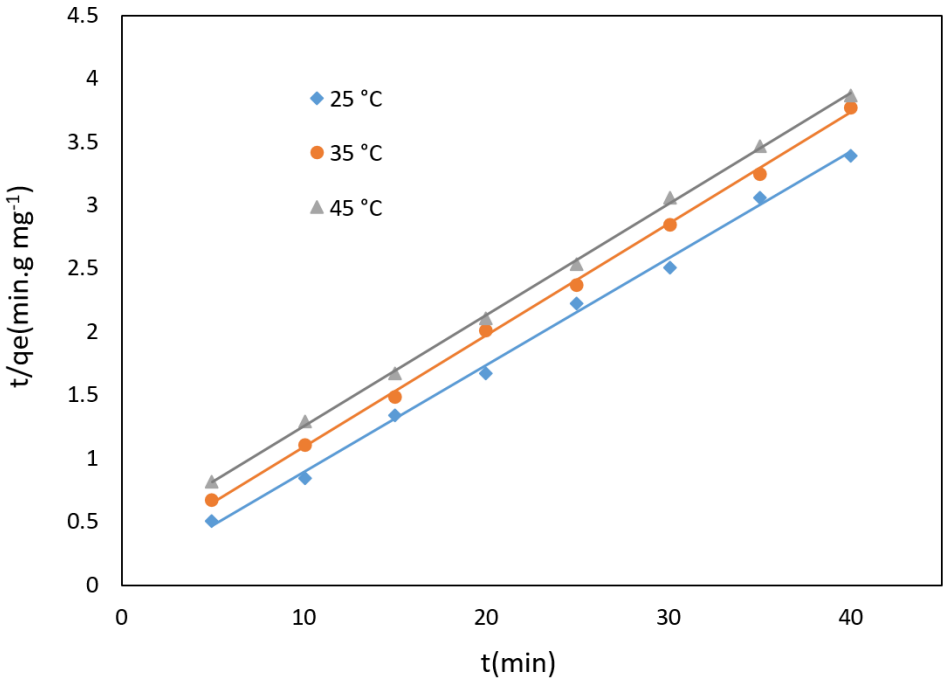

Fig. 10. Plot of the pseudo-second-order model of the CV-MP system.

Table 2. Kinetic parameters for linear modeling of CV dye adsorption.

Parameters		Pseudo-first-order model			Pseudo-second order model		
T (°K)	q_{exp} (mg g^{-1})	q_{cal}	K_1	R^2	q_{cal}	K_2	R^2
298	19.60	0.94	0.11	0.92	19.23	0.75	0.999
308	19.40	0.90	0.10	0.91	19.06	0.73	0.999
318	19.26	0.89	0.09	0.93	18.86	0.40	0.999

3.3.3.Intra-particle diffusion model

The graph below illustrates the variation in the quantity of dye adsorbed with each increase in time (qt) to the square root of time ($t^{½}$). The graph (Fig. 11) shows the results obtained using linear models of the intraparticle diffusion model. The kinetic parameters, derived from the gradients and ordinates of the theoretical lines, are presented in Table 3. Considering these results, the curves showing qe = f($t^{0.5}$) do not meet the origin, suggesting that diffusion of dye into the biomass pores is not the only mechanism determining adsorption kinetics. The double linearity of the curves indicates a combination of two distinct steps. The kinetic adsorption rate, therefore, varies from one stage to the next. Table 3 shows that the diffusion rate constant (K_d) values for the first stage are higher than those for the second stage, suggesting that the first stage of dye diffusion kinetics is much faster than the second. The first step represents the dyes' diffusion at the adsorbent's outer surface. In contrast, the second step reflects the diffusion of the dye molecules through the inner pores of the biomass particles, a relatively slower process. In addition, the non-zero values of the constant C indicate that the rate of adsorption of the CV onto the adsorbent is influenced by factors other than simple intraparticle diffusion [31].

.

3.4. Thermodynamic parameters

By employing the description of the fluctuation of ln(Kc) as a function of 1/T, the thermodynamic parameters of CV adsorption by MP are optimized. Table 4 shows the thermodynamic variables involved in the adsorption of CV onto MP. The thermodynamic parameters of CV biosorption on biomass are presented in Table 4 and Figure 12. The R^2 value for the linear fit was close to 1, indicating a good correlation. The negative value of the enthalpy change (ΔH°) indicates that biosorption processes are exothermic. Furthermore, the magnitude of ΔH° suggests that physical interactions are involved in these biosorption processes [38]. The positive value of ΔS° indicates an increase in the random character at the solid solution interface in the internal structure of CV adsorption on the biosorbent [24]. The negative values of ΔG° were observed at all three temperatures, indicating that the process is spontaneous and favored at these temperatures [39]. Other authors have also obtained this thermodynamic behavior [4].

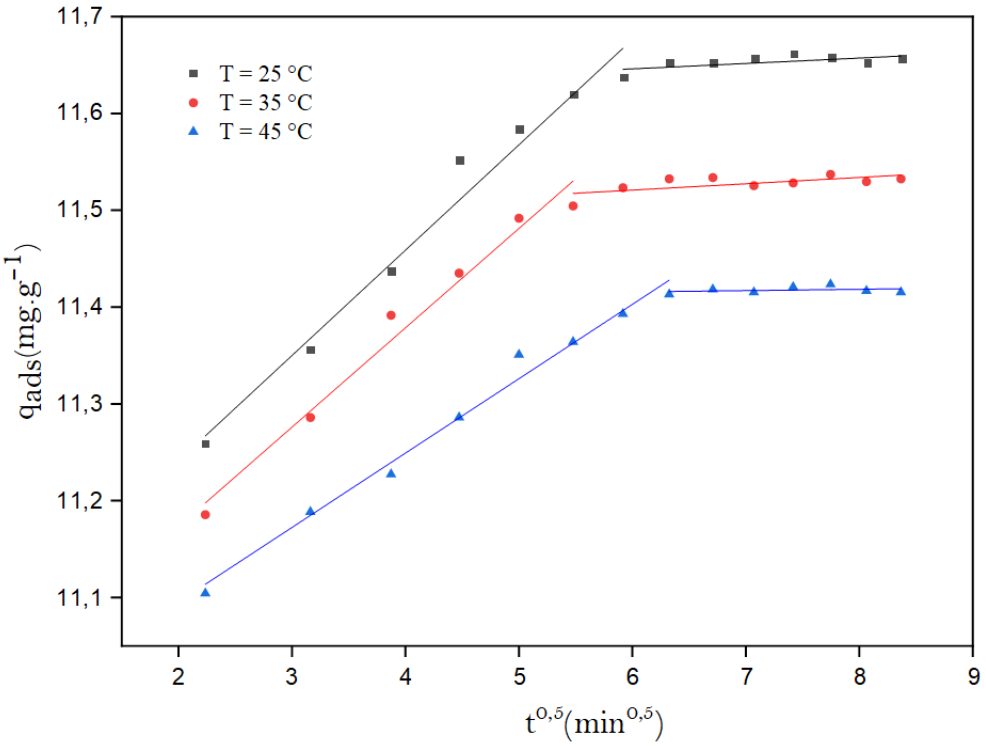

Fig. 11. Plot of the external diffusion model of the CV-MP system

Table 3. Parameters of the CV intra-particle diffusion model on MP

	1st right			2nd right		
T(°K)	C_1	K_1	R^2	C_2	K_2	R^2
298	11.02	0.11	0.97	11.61	0.05	0.98
308	10.96	0.10	0.98	11.48	0.06	0.99
318	10.94	0.11	0.98	11.40	0.01	0.99

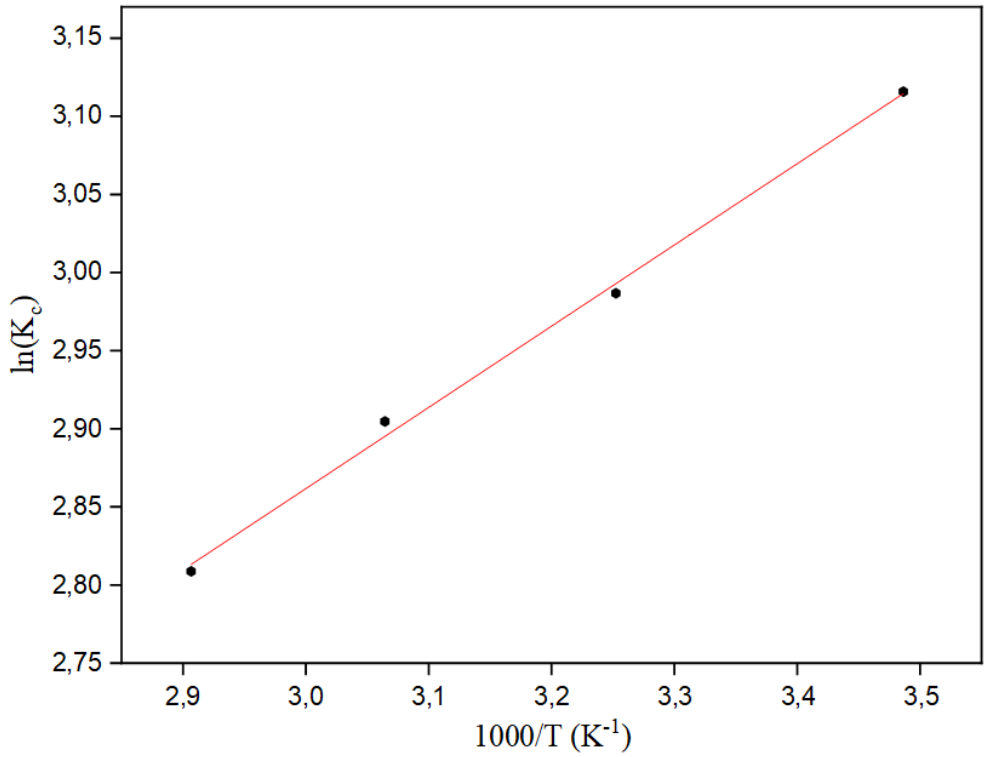

Fig. 12. The fluctuation of ln (K_c) as a function of 1/T in the adsorption of CV onto MP

Table 4. The thermodynamic parameters

Temperature (°K)	$\Delta H°_{ads}$ (Kj mol^{-1})	$\Delta S°_{ads}$ (j K^{-1} mol^{-1})	$\Delta G°_{ads}$ (Kj mol^{-1})	R^2
298	-4.32	10.80	-3.22	0.998
303			-3.27	
308			-3.33	
313			-3.38	

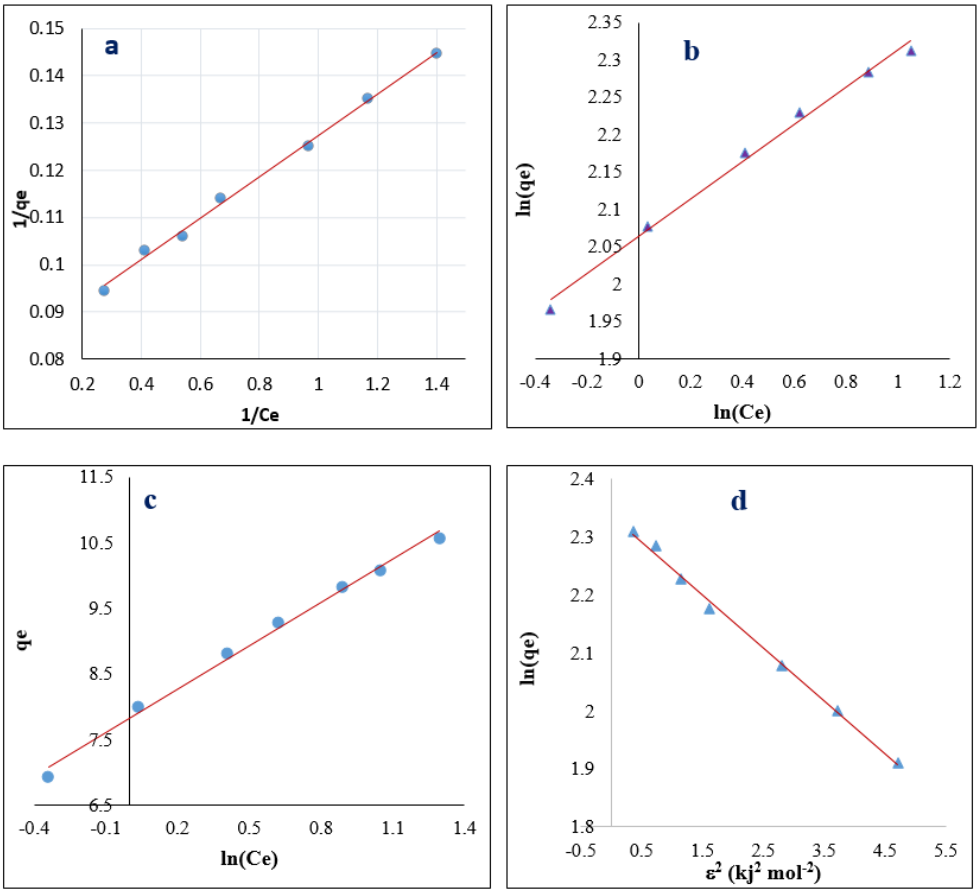

Fig. 13. (a) Langmuir isotherm, (b) Freundlich isotherm, (c) Temkin isotherm, (d) D-R Isotherm models for the biosorption of CV by MP

Table 5. Parameters of four adsorption isotherm models for CV by MP.

Isotherms	Parameters	Values
Langmuir	K_L	1.92
	q_{max}	11.95
	R_L	0.02
	R^2	0.99
Freundlich	K_f	7.87
	n	4.01
	R^2	0.998
Temkin	A_T	34.81
	b_T	1126.17
	R^2	0.99
D–R	q_D (mg g^{-1})	10.28
	β ($mol^2 kj^{-2}$)	0.126
	E (kj mol^{-1})	2.34
	R^2	0.99

3.5. Modeling of adsorption isotherm

The results of CV biosorption on MP were fitted to Langmuir, Freundlich, Temkin, and Dubinin-Radushkevich (D-R) isothermal models. The linear plots and parameters of these isothermal models are shown in Figure 13 and Table 5.

The Langmuir isotherm model characterizes the experimental results for CV biosorption on biomass. The high coefficient of determination value (R^2 = 0.984; Fig. 13a, Table 5) supports this, indicating that the biosorption process occurred in a monolayer. Furthermore, CV ions (K_L = 1.92 L mg^{-1}) significantly enhanced the biosorption sites on the biomass surface, indicating that they may efficiently extract dye particles from aqueous solutions [4]. The Langmuir isotherm model's second component, the dimensionless factor R_L, is determined by accounting for deviations from the linearity of biosorption. When R_L is within a range of zero and one, it indicates favorable biosorption [40]. According to the Freundlich model, the higher R^2 value of 0.998 proves that the Freundlich isothermal model accurately illustrates the equilibrium of CV biosorption by the biomass. This model was evaluated as a function of adsorption capacity (K_F) and adsorption intensity (n). This study found a KF value of 7.87 mg g-1, indicating a high biomass biosorption capacity for the CV dye (Table 5; Fig. 13 b) [4]. The adsorption intensity (n = 4,01) shows high biomass biosorption, suggesting that MP biomass adsorbs CV favorably and generates much stronger bonds, suggesting a chemisorption process [41]. The Temkin model is deemed appropriate for the biosorption of CV on biomass, as indicated by the high R^2 value of 0.998 (Fig. 13c), which matches the results presented in Table 5 [42]. This further supports the idea of heterogeneous locations with various binding energies. As a result of the lower adsorption heat of ions in the layer, the increased b_T value (1.126 kJ mol^{-1}) indicates a strong interaction between CV ions and various functional groups on the biomass surface [37]. Moreover, the Temkin (b_T) model adsorption energy of the dye from the aqueous solution is positive, indicating an exothermic character of the adsorption [43]. The high R^2 value of 0.998 (Fig. 13d) of the D-R models demonstrates that it is a good fit for the biosorption of CV onto biomass, as indicated by the data in Table 5. Table 5 also presents the computed D-R isotherm coefficients. The E value is typically utilized to evaluate the type of adsorption. A physisorption process has an E value less than 8.0 kJ mol^{-1}, whereas an ion exchange process has an E value between 8.0 and 16.0 kJ mol^{-1} [26]. The E value in this investigation was less than 8.0 kJ mol^{-1}, indicating that physisorption rather than adsorption was the mode of CV adsorption on biomass. Given the previously mentioned data, the biosorption process is most likely multilayer physisorption and multi-mechanistic, as indicated by the R^2 values of the Dubinin-Radushkevich, Freundlich, Langmuir, and Temkin biosorption isotherms, all of which exceed 0.98.

3.6. Mechanism of CV adsorption on MP

Essential analyses, such as Fourier transform infrared spectroscopy, are required to suggest a mechanism for CV adsorption onto PM. Before and after CV adsorption, these analyses allow us to study the interaction between the dye molecules and the active sites on the surface of the solid material. A study of the biomass before and after biosorption of the BM dye onto the PM surface is revealed using scanning electron microscopy (SEM) (Figures 14A and B). A highly porous cell wall is observed in the solid, with changes in porosity reported in association with dye biosorption. Furthermore, by comparing the Fourier transform infrared (FTIR) spectra of the solid material before and after adsorption of the dye (Fig. 15), it is observed that the structure and walls of the solid material, mainly composed of cellulose, hemicellulose, and lignin, contain various functional groups. Analysis of the spectra shows a notable variation in the peaks at 3335 cm^{-1} and 1600 cm^{-1}, indicating that the dye has adsorbed onto the surface of the biosorbent. In addition, the intensity of the peaks at 1724 cm^{-1} and 1590 cm^{-1} decreased. The areas between 1777-1183 cm^{-1} and 1136-734 cm^{-1} also underwent significant

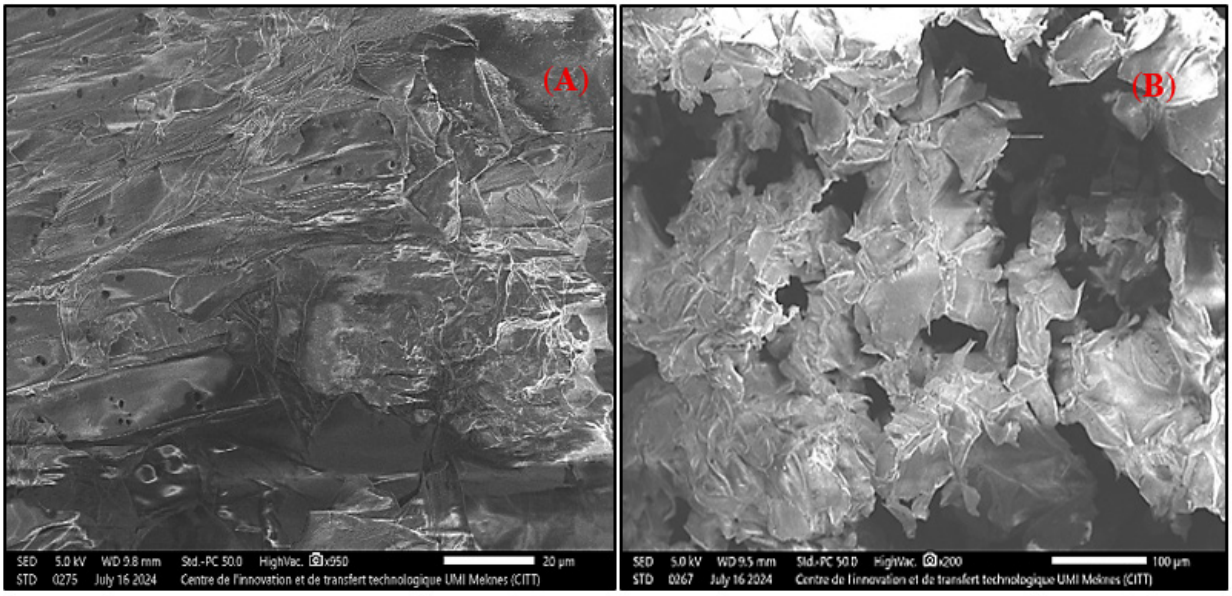

Fig. 14. SEM of raw PM (A) before and (B) after the CV biosorption.

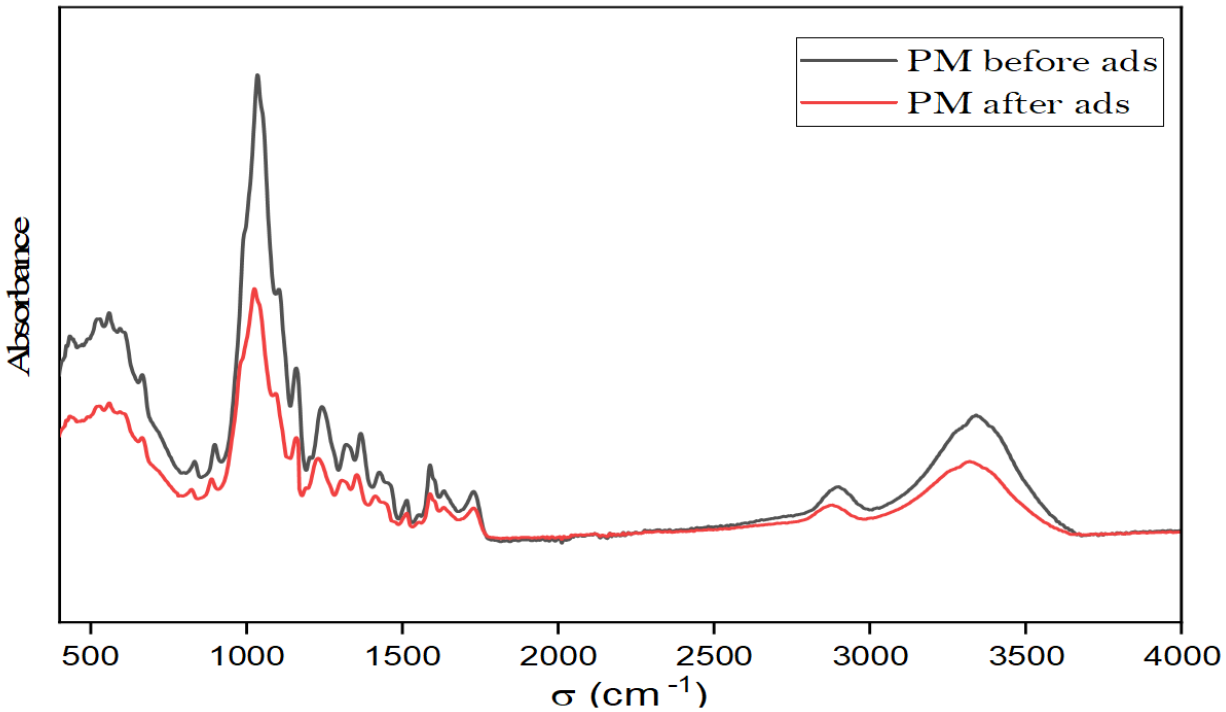

Fig. 15. FT-IR spectrum of raw PM and after adsorption of dye molecules.

shifts, without any new bands appearing. These observations suggest that electrostatic interactions or hydrogen bonds are involved in the adsorption process, indicating physisorption of the dye onto the particles.

4. Conclusion

The current study demonstrated that maize pith can be used effectively and economically as a biosorbent for removing crystal violet dye. Various parameters, such as contact time, biosorbent mass,

system temperature, and pH, were investigated. Four isotherms and kinetic models were applied to simulate the biosorption process. Langmuir, Freundlich, Dubinin-Radushkevich, and Temkin models were used for the isotherms. In contrast, the kinetics were modeled mainly by the pseudo-second-order model, which showed a higher coefficient of determination. The intraparticle diffusion model was employed to analyze the rate of progression of the CV biosorption process, revealing that smaller particles had a greater influence on the boundary layer. Thermodynamic parameters indicated exothermic, random, and spontaneous biosorption of CV, underlining the biosorption mechanism. FTIR analysis revealed that biosorption of CV dye onto biomass involved hydrogen bonding, electrostatic interactions, and ion exchange. Thus, maize pith proved to be an effective and economical biosorbent for the adsorption of hazardous textile dyes from aqueous solutions and wastewater.

5. Acknowledgements

The author would like to thank the Laboratory of Chemistry and Biology Applied to the Environment, Faculty of Sciences, Morocco.

6. References

[1] G. Y. Abate, A. N. Alene, A. T. Habte, D. M. Getahun, Adsorptive removal of malachite green dye from aqueous solution onto activated carbon of Catha edulis stem as a low cost bio-adsorbent, Environ. Syst. Res., 9 (2020) 29. https://doi.org/10.1186/s40068-020-00191-4

[2] M. Bilal, Mitigation of environmentally-related hazardous pollutants from water matrices using nanostructured materials – A review, Chemosphere, 253 (2020) 126770. https://doi.org/10.1016/j.chemosphere.2020.126770

[3] J. Rakhtshah, H. Shirkhanloo, N. Esmaeili, A rapid extraction of toxic styrene from water and wastewater samples based on hydroxyethyl methylimidazolium tetrafluoroborate immobilized on MWCNTs by ultra-assisted dispersive cyclic conjugation-micro-solid phase extraction, Microchem. J., 170 (2021) 106759. https://doi.org/10.1016/j.microc.2021.106759

[4] M. A. Fawzy, Sustainable use of marine macroalga sargassum muticum as a biosorbent for hazardous crystal violet dye: Isotherm, kinetic and thermodynamic modeling, Sustainability, 15 (2023) 15064. https://doi.org/10.3390/su152015064

[5] M. Ouchabi, P. S. Abdullah, H. Lgaz, Y. Cho, F. Boukhlifi, comparative study on adsorption of crystal violet and chromium (VI) by activated carbon derived from spent coffee grounds, Appl. Sci.,13 (2023) 985. https://doi.org/10.3390/app13020985

[6] M. M. Asl, N. Mansouri, S. Mirzahosseini, F. Atabi, Functionalized graphene oxide with bismuth and titanium oxide nanoparticles for efficiently removing formaldehyde from the air by photocatalytic degradation–adsorption process, J. Anal. Test., 7 (2023) 444–458. https://doi.org/10.1007/s41664-023-00272-0

[7] A. Faghihi-Zarandi, J. Rakhtshah, B. Bahrami Yarahmadi, A rapid removal of xylene vapor from environmental air based on bismuth oxide coupled to heterogeneous graphene/graphene oxide by UV photo-catalectic degradation-adsorption procedure, J. Environ. Chem. Eng., 8 (2020) 104193. https://doi.org/10.1016/j.jece.2020.104193

[8] S. Teimoori, H. Shirkhanloo, A. H. Hassani, M. Panahi, N. Mansouri, Rapid extraction of BTEX in water and milk samples based on functionalized multi-walled carbon nanotubes by dispersive homogenized-micro-solid phase extraction, Food Chem., 421 (2023) 136229. https://doi.org/10.1016/j.foodchem.2023.136229

[9] S. Teimoori, A. H. Hassani, M. Panahi, N. Mansouri, An immobilization of aminopropyl trimethoxysilane-phenanthrene carbaldehyde

on graphene oxide for toluene extraction and separation in water samples, Chemosphere, 316 (2023) 137800. https://doi.org/10.1016/j.chemosphere.2023.137800

[10] A. Faghihi-Zarandi, C. Jamshidzadeh, A new method for removal of hazardous toluene vapor from air based on ionic liquid-phase adsorbent, Int. J. Environ. Sci. Technol., 16 (2019) 2797–2808. https://doi.org/ 10.1007/s13762-018-1975-5

[11] I. A. Amar, E. A. Zayid, S. A. Dhikeel, M. Y. Najem, Biosorption removal of methylene blue dye from aqueous solutions using phosphoric acid-treated balanites aegyptiaca seed husks powder, Biointerface Res. Appl. Chem., 12 (2022) 7845–7862. https://doi.org/10.33263/BRIAC126.78457862

[12] H. Atlas, Sustainable biosorption of methylthioninium chloride in wastewaters using new cystoseira barbata seaweed: Equilibrium isotherm, kinetic modeling and mechanism analysis, Arab. J. Chem., 17 (2024) 105532. https://doi.org/10.1016/j.arabjc.2023.105532

[13] R. Ashouri, S.A. Hajiseyed Mirzahosseini, Synthesis of carbon quantum dots from olive stones for efficient adsorption of benzene from the ambient air, J. Nanostructures, 11 (2021) 480-497. https://doi.org/10.22052/JNS.2021.03.007

[14] A. Kali, Study of the adsorption properties of an almond shell in the elimination of methylene blue in an aquatic, Moroccan J. Chem., 10 (2022) 509–522. https://doi.org/10.48317/IMIST.PRSM/morjchem-v10i3.33140

[15] M. Sadoq, S. Imame, H. Atlas, Utilization of argan nut shells as a bioresource for efficient malachite green oxalate adsorption, Chem. Pap., 78 (2024) 7525–7540. https://doi.org/10.1007/s11696-024-03611-2

[16] M. Jabri, Valorization of lignocellulosic wastes material for efficient adsorption of a cationic azo dye and sludge recycling as a reinforcement of thermoplastic composite, Fluids, 8 (2023) 37. https://doi.org/10.3390/fluids8020037

[17] A. Salah Omer, Adsorption of crystal violet and methylene blue dyes using a cellulose-based adsorbent from sugercane bagasse: characterization, kinetic and isotherm studies, J. Mater. Res. Technol., 19 (2022) 3241–3254. https://doi.org/10.1016/j.jmrt.2022.06.045

[18] A. Kali, Efficient adsorption removal of an anionic azo dye by lignocellulosic waste material and sludge recycling into combustible briquettes, Colloids Interfaces, 6 (2022) 22. https://doi.org/ 10.3390/colloids6020022

[19] M. B. H. Abadi, J. Rakhtshah, Air pollution control: The evaluation of TerphApm@MWCNTs as a novel heterogeneous sorbent for benzene removal from air by solid phase gas extraction, Arab. J. Chem., 13 (2020) 1741-1751. https://doi.org/10.1016/j.arabjc.2018.01.011

[20] S. Teimoori, N. Mansouri, New extraction of toluene from water samples based on nano-carbon structure before determination by gas chromatography, Int. J. Environ. Sci. Technol., 20 (2023) 6589–6608. https://doi.org/10.1007/s13762-023-04906-9

[21] E. Sudova, J. Machova, Z. Svobodova, T. Vesely, Negative effects of malachite green and possibilities of its replacement in the treatment of fish eggs and fish: A review, Veterinarni Medicina, 52 (2007) 527–539. https://doi.org/ 10.17221/2027-VETMED

[22] A. Dehbi, Comparative study of malachite green and phenol adsorption on synthetic hematite iron oxide nanoparticles (α-Fe_2O_3), Surf. Interfaces, 21 (2020) 100637. https://doi.org/10.1016/j.surfin.2020.100637

[23] R Ashouri, Dynamic and static removal of benzene from air based on task-specific ionic liquid coated on MWCNTs by sorbent tube-headspace solid-phase extraction procedure, Int. J. Environ. Sci. Technol., 18 (2021) 2377-2390. https://doi.org/10.1007/s13762-020-02995-4

[24] S. Dawood, T. K. Sen, Removal of anionic

dye Congo red from aqueous solution by raw pine and acid-treated pine cone powder as adsorbent: Equilibrium, thermodynamic, kinetics, mechanism and process design, Water Res., 46 (2012) 1933–1946. https://doi.org/ 10.1016/j.watres.2012.01.009

[25] D. Kavitha, C. Namasivayam, Experimental and kinetic studies on methylene blue adsorption by coir pith carbon, Bioresour. Technol., 98 (2007) 14–21. https://doi.org/ 10.1016/j.biortech.2005.12.008

[26] Q. Du, Highly enhanced adsorption of congo red onto graphene oxide/chitosan fibers by wet-chemical etching off silica nanoparticles, Chem. Eng. J., 245 (2014) 99–106. https://doi.org/ 10.1016/j.cej.2014.02.006

[27] N. Esfandiar, B. Nasernejad,T. Ebadi, Removal of Mn(II) from groundwater by sugarcane bagasse and activated carbon (a comparative study): Application of response surface methodology (RSM), J. Ind. Eng. Chem., 20 (2014) 3726–3736. https://doi.org/ 10.1016/j.jiec.2013.12.072

[28] Z. Belala, M. Jeguirim, M. Belhachemi, F. Addoun, G. Trouvé, Biosorption of basic dye from aqueous solutions by date stones and Palm-Trees Waste: Kinetic, equilibrium and thermodynamic studies, Desalination, 271 (2011) 80–87. https://doi.org/ 10.1016/j.desal.2010.12.009

[29] L. Soldatkina, M. Zavrichko, Equilibrium, kinetic, and thermodynamic studies of anionic dyes adsorption on corn stalks modified by cetylpyridinium bromide, Colloids Interfaces, 3 (2019) 4. https://doi.org/ 10.3390/colloids3010004

[30] H. Gu, X. Gao, H. Zhang, K. Chen, L. Peng, Fabrication and characterization of cellulose nanoparticles from maize stalk pith via ultrasonic-mediated cationic etherification, Ultrason. Sonochem., 66 (2020) 104932. https://doi.org/ 10.1016/j.ultsonch.2019.104932

[31] M. Sadoq, Eliminating crystal violet from aqueous solution by adsorption on naturel polysaccharide: Kinetic, isotherm, thermodynamic studies and mechanism analysis, Arab. J. Chem., 17 (2024) 105453. https://doi.org/ 10.1016/j.arabjc.2023.105453

[32] M. A. Al-Ghouti, J. Li, Y. Salamh, N. Al-Laqtah, G. Walker, M. N. M. Ahmad, Adsorption mechanisms of removing heavy metals and dyes from aqueous solution using date pits solid adsorbent, J. Hazard. Mater., 176 (2010) 510–520. https://doi.org/ 10.1016/j.jhazmat.2009.11.059

[33] E. N. Bakatula, D. Richard, C. M. Neculita, G. J. Zagury, Determination of point of zero charge of natural organic materials, Environ. Sci. Pollut. Res., 25 (2018) 7823–7833. https://doi.org/ 10.1007/s11356-017-1115-7

[34] G. Crini, H. N. Peindy, F. Gimbert, C. Robert, Removal of C.I. Basic Green 4 (Malachite Green) from aqueous solutions by adsorption using cyclodextrin-based adsorbent: Kinetic and equilibrium studies, Sep. Purif. Technol., 53 (2007) 97–110. https://doi.org/ 10.1016/j.seppur.2006.06.018

[35] E. K. Guechi, O. Hamdaoui, Biosorption of methylene blue from aqueous solution by potato (Solanum tuberosum) peel: equilibrium modelling, kinetic, and thermodynamic studies, Desalin. Water Treat., 57(2016)10270–10285. https://doi.org/ 10.1080/19443994.2015.1035338

[36] F. A. Pavan, E. C. Lima, S. L. P. Dias, A. C. Mazzocato, Methylene blue biosorption from aqueous solutions by yellow passion fruit waste, J. Hazard. Mater., 150 (2008) 703–712. https://doi.org /10.1016/ j.jhazmat.2007.05.023

[37] M. Mohammadi Asl, N. Mansouri, S. A. R. Haji Seyed Mirzahosseini, F. Atabi, Simultaneity comparative evaluation of toluene removal from the air by adsorption and UV semi-degradation-based adsorption procedure, Int. J. Environ. Sci. Technol., 21 (2024) 6677-6694. https://doi.org/10.1007/s13762-024-05503-0

[38] K. D. Belaid, S. Kacha, Study of the kinetics and thermodynamics of the adsorption of a

basic dye on sawdust, J. Water Sci., 24 (2011) 131–144. https://doi.org/ 10.7202/1006107ar

[39] M. N. Bennani, Sustainable biosorption of methylthioninium chloride in wastewaters using new cystoseira barbata seaweed: Equilibrium isotherm , kinetic modeling and mechanism analysis, Arab. J. Chem., 17 (2024)105532. https://doi.org/ 10.1016/j.arabjc.2023.105532

[40] E. Kalkan, H. Nadaroglu, N. Celebi, H. Celik, E. Tasgin, Experimental study to remediate acid fuchsin dye using laccase-modified zeolite from aqueous solutions, Polish J. Environ. Stud., 24 (2015) 115–124. https://doi.org/ 10.15244/pjoes/23797

[41] C. M. Oloo, J. M. Onyari, W. C. Wanyonyi, J. N. Wabomba, V. M. Muinde, Adsorptive removal of hazardous crystal violet dye form aqueous solution using Rhizophora mucronata stem-barks: Equilibrium and kinetics studies, Environ. Chem. Ecotoxicol., 2 (2020) 64–72. https://doi.org/ 10.1016/j.enceco.2020.05.001

[42] H. Zeghache, S. Hafsi, N. Gherraf, Adsorption of organic dyes onto commercial activated carbon by using non-linear regression method, Environment Asia J., 12 (2019) 127–142. https://doi.org/ 10.14456/ea.2019.15

[43] P. Sampranpiboon, Equilibrium isotherm models for adsorption of zinc (II) ion from aqueous solution on pulp waste faculty of engineering, WSEAS Trans. Environ. Dev., 10 (2014) 35–47. https://wseas.com/journals/ead/